Journal of Sound and Vibration 588 (2024) 118515

Contents lists available at ScienceDirect

Journal of Sound and Vibration

journal homepage: www.elsevier.com/locate/jsvi

Efficient method for calculating sound radiation from a circular source in an infinite baffle

Krzysztof Szemela [a,*], Wojciech P. Rdzanek [a], Marek Pawelczyk [b], Li Cheng [c]

[a] University of Rzeszów, College of Natural Sciences, Institute of Physics, Prof. S. Pigonia 1, 35-310 Rzeszów, Podkarpackie, Poland
[b] Silesian University of Technology, Department of Measurements and Control Systems, Akademicka 16, 44-100 Gliwice, Poland
[c] Department of Mechanical Engineering, Hong Kong Polytechnic University, Hong Kong, China

ARTICLE INFO

Keywords:
Baffled circular sound source
Continuity equations
Sound power
Sound pressure
Numerical efficiency
Helmholtz equation in the spherical coordinate system

ABSTRACT

The numerically efficient solution describing the sound radiation from a circular source located in a flat, rigid baffle is obtained. For this purpose, a half-space was divided into two subregions coupled through continuity equations. The Helmholtz equation was solved in both subregions. The proposed method can be used for circular baffled sources in the case when fluid–structure interactions are included, as well as for an input from a waveguide or cavity. The validity and numerical efficiency of the presented solution were tested assuming that a clamped circular plate is a source. The numerical simulations show that the results given by the proposed method agree with those given by the known integral solution. The exceptions are the field points at which the integral formulas fail and provide incorrect values of the sound pressure. Hence, the presented formulas can be the only method to perform accurate calculations at troublesome field points. The numerical efficiencies of the obtained formulas and integral ones were compared by estimating the value of the appropriate time ratios. The numerical analysis shows that the proposed method can be used to significantly improve calculations of the sound power and the sound pressure.

1. Introduction

Vibrating baffled planar surfaces very often generate acoustic waves. Therefore, there are many studies focused on predicting the sound radiation from such structures. The sound radiation of a set of circular pistons randomly placed on a flat baffle was calculated using Bouwkamp's impedance theorem [1]. The modal radiation efficiency of complex-shaped plates was obtained based on an equivalent piston model [2]. In this approach, each mode shape is approximated by a distribution of circular pistons oscillating in or out-of-phase.

Based on the discrete calculation method proposed by Hashimoto [3], the radiation matrix approach was developed to calculate the acoustic radiation from a baffled planar sound source [4,5]. This method can only be used at low frequencies because it requires dividing a sound source surface into elements much smaller than the wavelength.

The sound radiation of a baffled circular and elliptical radiator was predicted by dividing the vibrating surface into a finite number of small circular pistons [6,7]. The acoustic field of a vibrating baffled circular piston was obtained with the use of the series containing the integral of spherical Bessel functions [8]. Moreover, an efficient method to calculate the necessary integrals was proposed, employing a recurrence approach. The sound power radiated by a baffled circular plate was obtained by using the Rayleigh integral and integrating the acoustic intensity over a hemispherical surface [9]. Additionally, a low-frequency approximation was

* Corresponding author.
E-mail address: kszemela@ur.edu.pl (K. Szemela).

https://doi.org/10.1016/j.jsv.2024.118515
Received 8 January 2024; Received in revised form 13 May 2024; Accepted 14 May 2024
Available online 16 May 2024

presented for the radiation efficiency. The sound radiation from a baffled rectangular radiator was obtained based on the Rayleigh integral [10–12]. The spatial convolution method was used to solve the Rayleigh integral and provide numerically efficient formulas for the self and mutual radiation impedances of rectangular radiators located in a flat baffle [13]. Making use of the modified Fourier series and the Rayleigh–Ritz method, the sound power radiated by a baffled rectangular plate with elastically supported edges was found [14]. The acoustic radiation of a simply supported baffled rectangular plate excited by turbulent flow was predicted using the uncorrelated wall plane wave technique [15]. The vibro-acoustic response of the functionally graded lightweight square panel was investigated within the low and mid-frequency regions using the first-order shear deformation theory and finite element method [16].

Based on the Rayleigh integral, the acoustic field of a baffled circular piston was expressed as a series of spherical harmonics [17]. The series coefficients were given with the use of the recurrence formula. Then, by considering the special cases, the solution proposed by Hasegawa et al. was presented in simpler forms suitable for numerical computations [18]. Beranek and Mellow presented the formulas for the far-field acoustic pressure radiated by a shallow, spherical shell [19]. This solution can be modified to obtain the formulas describing the sound field generated by a flat plate in the case when fluid–structure interactions are included. Moreover, by using an analytical evaluation presented by Rdzanek [20] for an improper integral of a pair of Bessel functions, the obtained formulas can be expressed without the use of improper integrals. Based on the Bouwkamp's solution for the free space wave equation, the pressure field of a membrane in free space was presented in the form of multiple series [21]. Then, this method was used to obtain the formulas describing the sound radiation from a membrane located in an infinite baffle.

The formulas describing the sound radiation from a circular source were obtained by using the Hankel transform [22]. However, this solution, called the integral solution, is expressed by improper integrals and is not convenient for performing numerical calculations. To avoid difficulties caused by numerical integrations, some mathematical methods were proposed to conveniently calculate the coupling coefficients describing medium – structure interaction as well as the sound power. Making use of the Cauchy theorem on residues, the high-frequency asymptotic formulas for the coupling coefficients were obtained for a circular clamped plate [23]. This method was used to provide the high-frequency asymptotic formulas for the coupling coefficients in the case of an elastically supported circular and annular plate [24,25]. Using summations of multiple series containing the hypergeometric functions, the low-frequency asymptotic formulas for the real part of the coupling coefficients were presented for a simply supported circular plate and an elastically supported annular plate [26,27]. Based on the radial polynomials, the rapidly converging expansion series were obtained to calculate the coupling coefficients for a clamped circular and annular plate and for an elastically supported circular plate [28–30].

The presented literature review showed that the sound radiation from baffled sound sources is widely studied. The well-known integral solution describing the sound radiation from a circular clamped plate was presented in Appendices C and D. However, it is still needed to propose efficient and accurate methods for calculating the sound power and sound pressure radiated by baffled sources. Therefore, the main aim of this study is to propose a method for performing efficient and accurate calculations of the sound power and the sound pressure radiated by an arbitrary baffled circular source such as a membrane, a plate with different boundary configurations, or the outlet of a waveguide or cavity. The formulas for the sound pressure are obtained by dividing the half-space region into two subregions connected through continuity equations. The boundary between these subregions was a hemisphere that enclosed a sound source. The formulas given by the proposed method do not contain any improper integrals, and therefore, they can be highly numerically efficient for calculating the sound power as well as the sound pressure. Moreover, this approach, by eliminating some errors in numerical integrations, provides correct and accurate results.

2. Statement of the problem

The sound propagation is analyzed in a half-space. The sound source is a vibrating circular surface, called the source surface, located in an infinite, flat and perfectly rigid baffle. This source surface can be a planar sound source such as, e.g., a piston, membrane or plate, as well as an input from a circular waveguide or cavity. Therefore, the problem to be solved represents many practical cases. In order to describe the distribution of the acoustic pressure p, the spherical coordinate system (r,θ,φ) is introduced, where r is the radial distance, θ denotes the inclination angle, and φ is the azimuthal angle (see Fig. 1). It is assumed that the vibrating circular surface of the radius a is located in the plane $\theta=\pi/2$. The time harmonic processes with the time dependence $\exp(-i\omega t)$ are considered, where ω is the angular frequency. The linear theory of the acoustic field is employed, which means that the acoustic pressure satisfies the following Helmholtz equation

$$\Delta p(r,\theta,\varphi)+k^2 p(r,\theta,\varphi)=0 \tag{1}$$

where Δ is the Laplace operator in the spherical coordinate system, k is the acoustic wavenumber. Additionally, the following boundary condition

$$\left.\frac{\partial p}{\partial\theta}\right|_{\theta=\pi/2}=\begin{cases}-i\omega\rho r v(r',\varphi) & \text{for} \quad r<a\\ 0 & \text{for} \quad r\geq a\end{cases}, \tag{2}$$

must be satisfied, where ρ is the medium density and $v(r',\varphi)$ is the distribution of the normal component of the vibration velocity on the source surface in the polar coordinate system (r',φ). It should be noted that the coordinate r' is equivalent to the spherical coordinate r at the source points.

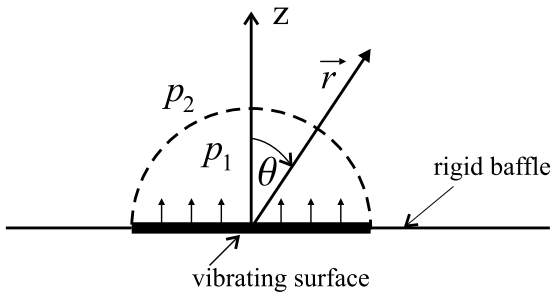

Fig. 1. A vibrating circular source of the radius a in a rigid baffle in the spherical coordinate system with the leading vector $\vec{r}$ and the inclination angle θ. The considered subregions: the first one for $r < a$ and the second one for $r \geq a$.

The transverse deflection of the circular source surface $W(r', \varphi)$ can be expressed in the form given by Eq. (D.2) where the eigenfunctions $\tilde{W}_{m,q}(r', \varphi)$ are related to the considered sound source. Then, the distribution of the vibration velocity $v(r', \varphi)$ can be written as

$$v(r', \varphi) = -i\omega \sum_{m=-M}^{M} \sum_{q=0}^{Q} c_{m,q} W_{|m|,q}(r') e^{im\varphi}. \tag{3}$$

where $c_{m,q}$ are constants to determine and M and Q are the truncation integers, which will be determined numerically to assure required accuracy (cf. Numerical Analysis herein).

The considered region extends to infinity, hence, the sound pressure must satisfy the Sommerfeld radiation conditions

$$\lim_{r\to\infty} \left[r \left(\frac{\partial p}{\partial r} - ikp \right) \right] = 0. \tag{4}$$

The solution of the considered problem is the function p which satisfies the Helmholtz equation Eq. (1) and the conditions from Eqs. (2) and (4).

3. Analytical solution for sound pressure

In order to solve the considered problem, the half-space region is divided into two subregions: subregion 1, for which $r < a$, $0 \leq \theta \leq \pi/2$ and $0 \leq \varphi < 2\pi$ and subregion 2, for which $r \geq a$, $0 \leq \theta \leq \pi/2$ and $0 \leq \varphi < 2\pi$ (see Fig. 1).

It is assumed that $p_1(r, \theta, \varphi)$ and $p_2(r, \theta, \varphi)$ describe the sound pressure distribution for subregions 1 and 2, respectively. It is necessary to find the appropriate functions describing the quantities p_1 and p_2. Furthermore, it should be noted that both solutions p_1 and p_2 must satisfy the Helmholtz equation from Eq. (1) and p_2 must satisfy the radiation condition from Eq. (4). Additionally, the boundary condition from Eq. (2) indicates that the solutions p_1 and p_2 must satisfy the following conditions

$$\left. \frac{\partial p_1}{\partial \theta} \right|_{\theta=\pi/2} = -i\omega\rho r v(r, \varphi), \tag{5}$$

and

$$\left. \frac{\partial p_2}{\partial \theta} \right|_{\theta=\pi/2} = 0. \tag{6}$$

Moreover, the following continuity conditions

$$\left. \frac{\partial p_1}{\partial r} \right|_{r=a} = \left. \frac{\partial p_2}{\partial r} \right|_{r=a}, \tag{7}$$

$$p_1(a, \theta, \varphi) = p_2(a, \theta, \varphi), \tag{8}$$

have to be satisfied.

The following solutions

$$\begin{aligned} p_1(r, \theta, \varphi) &= \sum_{m=-M}^{M} \sum_{l,n=0}^{N} \vartheta_{m,l,n} j_{|m|+2l}(\gamma_{|m|+2l,n} r/a) Y_{2l}^{m}(\theta, \varphi) \\ &+ \sum_{m=-M}^{M} \sum_{n=0}^{N} A_{m,n} j_{|m|+1}(\gamma_{|m|+1,n} r/a) Y_{1}^{m}(\theta, \varphi) + \sum_{m=-M}^{M} \sum_{l=0}^{N} B_{m,l} j_{|m|+2l}(r/a) Y_{2l}^{m}(\theta, \varphi), \end{aligned} \tag{9}$$

$$p_2(r, \theta, \varphi) = \sum_{m=-M}^{M} \sum_{l=0}^{N} D_{m,l} h_{|m|+2l}(kr) Y_{2l}^{m}(\theta, \varphi), \tag{10}$$

are proposed where N is the truncation integer, $j_\nu(\cdot)$ and $h_\nu(\cdot)$ denote the spherical Bessel function of the ν-th order and the spherical Hankel function of the first kind and ν-th order, respectively, the prime symbol denotes the derivative operation, and $\gamma_{\nu,n}$ is the eigenvalue for the following Neumann boundary condition $dj_\nu(\gamma_{\nu,n}r/a)/dr\big|_{r=a} = 0$, $n = 0,\dots,N$ is the ordinal number of the eigenvalue, $Y_\nu^m(\theta,\varphi) = P_{|m|+\nu}^{|m|}(\cos(\theta))\,e^{im\varphi}$, $P_\nu^{|m|}(\cdot)$ is the associated Legendre polynomial defined by Eq. (B.2) and $D_{m,l} = B_{m,l}j'_{|m|+2l}(1)/[kah'_{|m|+2l}(ka)]$, $\vartheta_{m,l,n}$, $A_{m,n}$, $B_{m,l}$ are constants to find. The solution given by Eq. (9) consists of the three parts. The first one, in the form of the triple sum, allows the sound pressure p_1 to satisfy the Helmholtz equation. The series with the constants $A_{m,n}$ and the series with the constants $B_{m,l}$ are superimposed on the former to satisfy the boundary conditions in Eqs. (5) and (8), respectively. It should be noted that the same truncation integer M is used in the presented solutions and in the solution of the equation of motion given by Eq. (3). All the necessary values of $\gamma_{\nu,n}$ are numerically calculated, and it is assumed that $\gamma_{0,0} = 0$. The acoustic pressure p_2 satisfies the Helmholtz equation as well as the Sommerfeld radiation condition. Taking into account that $P'^{|m|}_{|m|+2\nu}(0) = 0$ for $\nu \geq 0$ and $P'^{|m|}_{|m|+1}(0) \neq 0$, it can be noted that the acoustic pressure p_2 satisfies the condition from Eq. (6) and $\partial p_1/\partial\theta\big|_{\theta=\pi/2} \neq 0$. Moreover, the proposed solutions satisfy the continuity condition from Eq. (7).

Inserting the solution from Eqs. (9) into the boundary condition given by Eq. (5) and using Eq. (3) leads to

$$\sum_{n=0}^{N} A_{m,n}j_{|m|+1}(\gamma_{|m|+1,n}r/a)u_{|m|} = \omega^2\rho\sum_{q=0}^{Q} c_{m,q}rW_{|m|,q}(r), \tag{11}$$

where

$$u_{|m|} = P'^{|m|}_{|m|+1}(0) = \frac{(-1)^{|m|}(2|m|+2)!}{2^{|m|+1}(|m|+1)!}. \tag{12}$$

The values of $u_{|m|}$ were calculated based on the Rodrigues formula given by Eq. (B.2). Then, making use of the orthogonality of the spherical Bessel functions, the constants $A_{m,n}$ can be expressed as

$$A_{m,n} = \omega^2\rho a\sum_{q=0}^{Q} c_{m,q}\alpha_{|m|,n,q}, \tag{13}$$

where

$$\alpha_{|m|,n,q} = \frac{\int_0^1 W_{|m|,q}(aw)j_{|m|+1}(\gamma_{|m|+1,n}w)w^3dw}{u_{|m|}N_{|m|+1,n}}, \tag{14}$$

$$N_{\nu,n} = \frac{1}{a^3}\int_0^a j_\nu^2(\gamma_{\nu,n}r/a)r^2dr = \begin{cases} 1/3 \quad \text{for} \quad \nu = n = 0 \\ \dfrac{\pi}{4\gamma_{\nu,n}}\left[J^2_{\nu+1/2}(\gamma_{\nu,n}) - J_{\nu-1/2}(\gamma_{\nu,n})J_{\nu+3/2}(\gamma_{\nu,n})\right] \quad \text{otherwise.} \end{cases} \tag{15}$$

In the case of a planar circular sound source such as a membrane or plate, the function $W_{|m|,q}(aw)$ does not depend on the value of the sound source radius a. Thus, the coefficients $\alpha_{|m|,n,q}$ depend only on the eigenfunctions' shapes. Hence, the values of $\alpha_{|m|,n,q}$ can be calculated and stored in the computer's memory for the analyzed kind of sound source.

Inserting solutions from Eqs. (9) and (10) into the continuity condition from Eq. (8) results in

$$\sum_{n=0}^{N}\vartheta_{m,l,n}j_{|m|+2l}(\gamma_{|m|+2l,n}) + B_{m,l}\Psi_{|m|+2l} = -L_{|m|,l}\sum_{n=0}^{N}A_{m,n}j_{|m|+1}(\gamma_{|m|+1,n}), \tag{16}$$

where $\Psi_\nu = j_\nu(1) - h_\nu(ka)j'_\nu(1)/\left(kah'_\nu(ka)\right)$, $L_{|m|,l} = Y_{|m|,l}/M_{|m|,l}$,

$$M_{|m|,l} = \int_0^{\pi/2}\left(P^{|m|}_{|m|+2l}(\cos\theta)\right)^2\sin\theta d\theta = \frac{(2|m|+2l)!}{(2|m|+4l+1)(2l)!} \tag{17}$$

(see [31]) and

$$Y_{|m|,l} = \int_0^{\pi/2} P^{|m|}_{|m|+1}(\cos\theta)P^{|m|}_{|m|+2l}(\cos\theta)\sin\theta d\theta. \tag{18}$$

The coefficients $Y_{|m|,l}$ are independent constants. The correct values of $Y_{|m|,l}$ cannot be obtained by using the procedures of numerical integration when l assumes some greater values. This is due to the fact that the integrand in Eq. (18) strongly oscillates around zero. To avoid this difficulty, the analytical formulas for calculating accurate values of these coefficients are obtained and presented in Appendix B.

The values of the constants $\vartheta_{m,l,n}$ should be assumed so that the solution p_1 can satisfy the Helmholtz equation. Inserting the solution from Eq. (9) into Eq. (1) yields

$$\begin{aligned}\sum_{l=0}^{N}\Bigg[\sum_{n=0}^{N}\vartheta_{m,l,n}j_{|m|+2l}(\gamma_{|m|+2l,n}r/a)\left(k^2a^2-\gamma_{|m|+2l,n}^2\right)+\\ B_{m,l}\,j_{|m|+2l}(r/a)\left(k^2a^2-1\right)\Bigg]P_{|m|+2l}^{|m|}(\cos\theta)=\\ -\sum_{n'=0}^{N}A_{m,n'}\,j_{|m|+1}(\gamma_{|m|+1,n'}r/a)\left(k^2a^2-\gamma_{|m|+1,n'}^2\right)P_{|m|+1}^{|m|}(\cos\theta).\end{aligned}\tag{19}$$

Then, by using the orthogonality of the Legendre polynomials $P_{|m|+2l}^{|m|}(\cos\theta)$ and the orthogonality of the functions $j_{|m|+2l}(\gamma_{|m|+2l,n}r/a)$, the following formula can be written

$$\begin{aligned}\vartheta_{m,l,n}=-\Lambda_{|m|+2l,n}\Bigg[B_{m,l}\left(k^2a^2-1\right)X_{|m|+2l,n}+\\ L_{|m|,l}\sum_{n'=0}^{N}A_{m,n'}\left(k^2a^2-\gamma_{|m|+1,n'}^2\right)G_{|m|,l,n,n'}\Bigg],\end{aligned}\tag{20}$$

where $\Lambda_{\nu,n}=1/\left[N_{\nu,n}\left(k^2a^2-\gamma_{\nu,n}^2\right)\right]$,

$$X_{\nu,n}=\int_0^1 j_\nu(w)j_\nu(\gamma_{\nu,n}w)w^2dw,\tag{21}$$

and

$$G_{|m|,l,n,n'}=\int_0^1 j_{|m|+2l}(\gamma_{|m|+2l,n}w)j_{|m|+1}(\gamma_{|m|+1,n'}w)w^2dw.\tag{22}$$

The analytical formula for coefficients $X_{\nu,n}$ is presented in Appendix A. The coefficient $G_{|m|,l,n,n'}$ can be calculated based on numerical procedures. However, it should be noted that the values $X_{\nu,n}$ and $G_{|m|,l,n,n'}$ are independent constants that can be calculated once and stored in a computer's memory.

By inserting Eq. (20) into Eq. (16) and using Eq. (13), the constants $B_{m,l}$ can be expressed as

$$B_{m,l}=\omega^2\rho a\sum_{q=0}^{Q}c_{m,q}\beta_{|m|,l,q},\tag{23}$$

where

$$\begin{aligned}\beta_{|m|,l,q}=K_{|m|,l}\sum_{n=0}^{N}\alpha_{|m|,n,q}[(k^2a^2-\gamma_{|m|+1,n}^2)R_{|m|,l,n}\\ -j_{|m|+1}(\gamma_{|m|+1,n})],\end{aligned}\tag{24}$$

$$K_{|m|,l}=\frac{L_{|m|,l}}{\Psi_{|m|+2l}-(k^2a^2-1)V_{|m|+2l}},\tag{25}$$

$$R_{|m|,l,n}=\sum_{n'=0}^{N}\Lambda j_{|m|+2l,n'}G_{|m|,l,n',n},\tag{26}$$

$$V_\nu=\sum_{n=0}^{N}\Lambda j_{\nu,n}X_{\nu,n}\tag{27}$$

and $\Lambda j_{\nu,n}=\Lambda_{\nu,n}j_\nu(\gamma_{\nu,n})$. Combining Eqs. (13), (20) and (23) results in

$$\vartheta_{m,l,n}=\omega^2\rho a\sum_{q=0}^{Q}c_{m,q}T_{|m|,l,n,q},\tag{28}$$

where

$$\begin{aligned}T_{|m|,l,n,q}=-\Lambda_{|m|+2l,n}[\left(k^2a^2-1\right)X_{|m|+2l,n}\beta_{|m|,l,q}+\\ L_{|m|,l}\sum_{n'=0}^{N}\left(k^2a^2-\gamma_{|m|+1,n'}^2\right)G_{|m|,l,n,n'}\alpha_{|m|,n',q}].\end{aligned}\tag{29}$$

After calculating constants $c_{m,q}$ from the set of equations given by Eq. (D.11), the values of constants $\vartheta_{m,l,n}$, $A_{m,n}$ and $B_{m,l}$ can be found using Eqs. (13), (23) and (28). Then, the sound pressure distribution in the half-space can be calculated from the solutions given by Eqs. (9) and (10).

4. Formula for calculating the coupling coefficients

The values of coupling coefficients $\xi_{|m|,q,q'}$ are necessary to calculate constants $c_{m,q}$ from the set of equations given by Eq. (D.11). These coefficients are expressed with the use of the improper integral given by Eq. (D.12). Hence, the values of $\xi_{|m|,q,q'}$ can be found only by using numerical procedures which is troublesome as well as time-consuming, especially in the case of improper integrals. Moreover, the numerical procedures can produce some numerical errors. This means that the values obtained from Eq. (11) can be inaccurate or even incorrect.

To overcome all these difficulties related to the use of the integral formula from Eq. (D.12), the proposed solution from Eq. (9) is used to obtain an efficient formula for calculating the coefficients $\xi_{|m|,q,q'}$. For this purpose, the pressure on the plate's surface $p_s(r',\varphi)$ must be expressed in a suitable form. It should be noted that on the sound source surface, when $\theta = \pi/2$, the cylindrical coordinate r' is equivalent to the spherical coordinate r and $p_s(r',\varphi) = p_1(r',\pi/2,\varphi)$. Then, using Eqs. (23) and (28) and taking into account that $P^{|m|}_{|m|+1}(0) = 0$ leads to

$$p_s(r',\varphi) = \omega^2\rho a \sum_{m=-M}^{M}\sum_{q=0}^{Q} c_{m,q}\left\{\sum_{l=0}^{N}\left[\left(\sum_{n=0}^{N} T_{|m|,l,n,q} j_{|m|+2l}(\gamma_{|m|+2l,n} r'/a) + \beta_{|m|,l,q} j_{|m|+2l}(r'/a)\right) P^{|m|}_{|m|+2l}(0)\right]\right\} e^{im\varphi}. \tag{30}$$

Based on Eqs. (30) and (D.8), it can be deduced that

$$p^{(r)}_{|m|,q}(r') = \omega^2\rho a \sum_{l=0}^{N}\left(\sum_{n=0}^{N} T_{|m|,l,n,q} j_{|m|+2l}(\gamma_{|m|+2l,n} r'/a) + \beta_{|m|,l,q} j_{|m|+2l}(r'/a)\right) P^{|m|}_{|m|+2l}(0). \tag{31}$$

Finally, inserting Eq. (31) into Eq. (D.10) results in

$$\xi_{|m|,q,q'} = 2i \sum_{l=0}^{N}\left(\sum_{n=0}^{N} T_{|m|,l,n,q'} \Omega_{|m|,q,l,n} + \beta_{|m|,l,q'} \varepsilon_{|m|,q,l}\right), \tag{32}$$

where

$$\Omega_{|m|,q,l,n} = P^{|m|}_{|m|+2l}(0) \int_0^1 j_{|m|+2l}(\gamma_{|m|+2l,n} w) W_{|m|,q}(aw) w\, dw, \tag{33}$$

and

$$\varepsilon_{|m|,q,l} = P^{|m|}_{|m|+2l}(0) \int_0^1 j_{|m|+2l}(w) W_{|m|,q}(aw) w\, dw. \tag{34}$$

The coefficients from Eqs. (33) and (34) can be calculated by using numerical integration procedures. However, taking into account that the integration limits are finite, these numerical procedures are not highly time-consuming, and their results are accurate enough . Moreover, it should be emphasized that the coefficients $\Omega_{|m|,q,l,n}$ and $\varepsilon_{|m|,q,l}$ depend only on the shape of sound source eigenfunctions, therefore, their values can be calculated once and stored in a computer's memory.

5. Hints to increase the numerical efficiency of the proposed solution

The numerical procedures should be properly implemented to efficiently calculate the sound radiation using the presented formulas. Therefore, some useful hints to improve numerical calculations are listed below.

1. The following coefficients: $\gamma_{\nu,n}$, $N_{\nu,n}$, $X_{\nu,n}$, $j_\nu(\gamma_{\nu,n})$, $L_{|m|,n}$, $u_{|m|}$, $P^{|m|}_{|m|+2n}(0)$ and $G_{|m|,l,n,n'}$ are independent constants, therefore, their values can be calculated once and then stored in a computer's memory.
2. After choosing a sound source, the shapes of eigenfunctions $W_{|m|,q}(r)$ are known, and the following coefficients: $\alpha_{|m|,n,q}$, $\Omega_{|m|,q,l,n}$ and $\varepsilon_{|m|,q,l}$ can also be calculated once and stored in a computer's memory.
3. The values of the associated Legendre polynomials can be calculated with the use of the following recurrence relation

$$l P^{|m|}_{|m|+l}(w) = (2|m|+2l-1) w P^{|m|}_{|m|+l-1}(w) - (2|m|+l-1) P^{|m|}_{|m|+l-2}(w), \tag{35}$$

   where the starting values are: $P^{|m|}_{|m|}(w) = (-1)^{|m|}(2|m|)!(1-w^2)^{|m|/2}/[2^{|m|}(|m|)!]$ and $P^{|m|}_{|m|+1}(w) = (2|m|+1) w P^{|m|}_{|m|}(w)$. This technique is much more efficient than calculating each value of $P^{|m|}_{|m|+2l}(w)$ separately.
4. Taking into account that the spherical Hankel function of the first kind $h_\nu(w) = j_\nu(w) + i y_\nu(w)$ where $y_\nu(\cdot)$ is the Neumann spherical function, the functions $j_\nu(w)$ and $h_\nu(w)$ for the fixed value of w can be calculated with the use of the following recurrence relations

$$wj_\nu(w) = (2\nu+3)j_{\nu+1}(w) - wj_{\nu+2}(w), \tag{36a}$$

$$wy_\nu(w) = (2\nu-1)y_{\nu-1}(w) - wy_{\nu-2}(w), \tag{36b}$$

where the starting values are: $j_{M+2N}(w)$, $j_{M+2N-1}(w)$ calculated by using the function implemented in the software for performing numerical calculations, and $y_0(w) = -\cos w/w$ and $y_1(w) = -(w\sin w + \cos w)/w^2$. To maintain the numerical stability, the values of the functions $j_\nu(w)$ and $y_\nu(w)$ are calculated by using descending and ascending recurrence relations, respectively.

5. A sum $\sum_{j=0}^{N} A_j B_j$ can be more quickly calculated as the following scalar product $\vec{A}\cdot\vec{B}$ where $\vec{A} = [A_0, A_1, \ldots, A_N]$, $\vec{B} = [B_0, B_1, \ldots, B_N]$ and the dot symbol denotes the scalar product operation. This is due to the fact that a software can use different memory access mechanisms for different mathematical operations. The calculation of a scalar product is a basic and well-optimized operation; hence, it can be performed very efficiently.
6. To efficiently obtain the sound pressure distribution for a fixed value of the frequency, the constants $\vartheta_{m,l,n}$, $A_{m,n}$ and $B_{m,l}$ can be calculated once and stored in a computer's memory.
7. The calculations of the sound pressure distribution for a given value of the coordinate θ can be improved by performing the preliminary calculations of the following values $P_{|m|+2l}^{|m|}(\cos\theta)$ and $P_{|m|+1}^{|m|}(\cos\theta)$ and storing their results in a computer's memory. The values of the Legendre polynomials can be efficiently obtained with the use of the recurrence formula from Eq. (35).
8. Additionally, to improve the calculations of the sound pressure at field points of different values of the coordinate $r \geq a$ and in the case when the values of the coordinates θ and φ are fixed, the solution from Eq. (10) can be transformed into a more efficient form for numerical calculations. For this purpose, the formula for the sound pressure p_2 can be rewritten as

$$p_2(r,\theta,\varphi) = \sum_{m=0}^{M}\sum_{l=0}^{N} \kappa_m h_{|m|+2l}(kr)\left[D_{m,l}Y_{2l}^{m}(\theta,\varphi) + D_{-m,l}Y_{2l}^{-m}(\theta,\varphi)\right], \tag{37}$$

where $\kappa_0 = 1/2$ and $\kappa_m = 1$ for $m > 0$. Then, the following summation index $u = m + 2l$ can be introduced, which leads to

$$p_2(r,\theta,\varphi) = \sum_{u=0}^{M+2N} h_u(kr)\Xi_u(\theta,\varphi), \tag{38}$$

where

$$\Xi_u(\theta,\varphi) = \sum_{l=l_1}^{l_2} \kappa_{u-2l}\left[D_{u-2l,l}Y_{2l}^{u-2l}(\theta,\varphi) + D_{-u+2l,l}Y_{2l}^{-u+2l}(\theta,\varphi)\right], \tag{39}$$

$l_1 = \max(0, \lceil (u-M)/2 \rceil)$, $l_2 = \min(N, \lfloor u/2 \rfloor)$, $\max(\nu,\mu)$ gives ν if $\nu > \mu$ and μ otherwise, $\min(\nu,\mu)$ gives ν if $\nu < \mu$ and μ otherwise, $\lceil \nu \rceil$ is the smallest integer greater than or equal to ν, $\lfloor \nu \rfloor$ gives the greatest integer less than or equal to ν.
In the case when the values of the coordinate θ and φ are fixed, the coefficients $\Xi_u(\theta,\varphi)$ can be calculated once and stored in a computer's memory. Then, the formula given by Eq. (38) can be used to efficiently calculate the sound pressure for different values of the coordinate r.
9. The sound pressure distribution for a given value of the coordinate $r < a$ can be efficiently found by performing the preliminary calculations of the following values: $j_{|m|+2l}(\gamma_{|m|+2l,n}r/a)$, $j_{|m|+1}(\gamma_{|m|+1,n}r/a)$ and $j_{|m|+2l}(r/a)$ and stored their results in a computer's memory. Moreover, the preliminary calculations of the values $h_{|m|+2l}(kr)$ can improve the calculations of the sound pressure distribution for a given value of $r \geq a$. The values of $j_{|m|+2l}(r/a)$ and $h_{|m|+2l}(kr)$ can be efficiently obtained with the use of the recurrence formula from Eq. (36).

The numerically efficient implementation of the proposed solution prepared in the Mathematica programming language with the use of the above hints can be found in the codes of the scripts provided on reasonable request.

6. Numerical analysis of sound radiation from a clamped circular plate in an infinite baffle

The main aim of the numerical analysis is to investigate the correctness and numerical efficiency of the proposed method. To validate the obtained formulas, the known integral solution for a clamped circular plate located in a flat, rigid baffle is used. The integral solution is presented in Appendices C and D. The simulations are performed assuming that the plate is excited by a point excitation given by

$$f(r',\varphi) = f_0\delta(r'-r_0')\delta(\varphi-\varphi_0)/r', \tag{40}$$

where f_0 is the excitation amplitude, $\delta(\cdot)$ is the delta Dirac function, and r_0' and φ_0 are the polar coordinates of the excited plate's point. Using Eq. (40), the modal excitation coefficients given by Eq. (D.7) can be calculated as $F_{m,q} = f_0\tilde{W}_{m,q}^{*}(r_0',\varphi_0)$. All the parameter values assumed in the numerical simulations are listed in Table 1.

The sound radiation of a baffled circular plate was investigated [24,29]. Therefore, this issue is not discussed. Instead, the numerical analysis is focused on testing the validity of the proposed method and comparing its numerical efficiency with the numerical efficiency of the integral solution.

Table 1
Values of the parameters used in the numerical calculations.

Parameter	Value
Sound speed in the medium	c=343 m/s
Density of the medium	$\rho = 1.21$ kg/m^3
Plate's radius	$a = 0.15$ m
Plate's Young modulus	$E = 210$ GPa
Plate's Poisson ratio	$\nu = 0.3$
Plate's density	$\rho_p = 7850$ kg/m^3
Plate's thickness	$h = 1$ mm
Plate's damping coefficient	$\eta = 10^{-4}$
Excitation's amplitude	$f_0 = 1$ N

Correct results can be obtained only when the values of the truncation integers M and Q are large enough. To estimate an inaccuracy caused by including only a finite number of terms in the sums, the following truncation error is defined

$$E_t = \frac{|A - A_{ref.}|}{|A_{ref.}|} \cdot 100\%, \tag{41}$$

where A is the analyzed value and $A_{ref.}$ is its reference value obtained by assuming instead of the truncation integers M, Q the reference truncation integers $\lceil\sqrt{2}M\rceil$ and $\lceil\sqrt{2}Q\rceil$ where $\lceil u\rceil$ denotes the smallest integer number greater than or equal to u. In the case of the sound pressure, the value of $A_{ref.}$ is calculated using about two times greater number of plate modes than the value A. Hence, the truncation error E_t precisely indicates the influence of the unaccounted plate's modes on the accuracy of the obtained results. This quantity is calculated to prove that the presented results are correct and accurate enough to be analyzed.

In order to validate the obtained solution, the results given by the presented formulas are compared with the results provided by the integral formulas. For this purpose, the following relative error

$$E = \frac{|\mu - \mu_I|}{|\mu_I|} \cdot 100\%, \tag{42}$$

is defined where μ and μ_I are the values of the analyzed quantity calculated with the use of the proposed formulas and the known integral solution, respectively.

The sound radiation of a clamped circular plate located in a flat, infinite and perfectly rigid baffle was analyzed by Rdzanek in [28]. Therefore, the numerical analysis performed in this study is focused on testing the accuracy and numerical efficiency of the proposed method. The results given by the presented solution are compared with those provided by the known integral formulas. The numerical efficiency of the proposed method is compared with the numerical efficiency of the integral formulas by estimating appropriate time ratios. The numerical simulations are performed with the use of the software Mathematica. To make the efficiency comparison reliable, all numerical integrations are performed using built-in procedures. It can be assumed that the procedures implemented in commercial software are as efficient as possible.

6.1. Efficiency of sound power calculations

The sound power radiated by a baffled circular plate can be calculated using the following formula

$$P = P_a - iP_r = \frac{\pi}{2}\omega^3 a^3 \rho \sum_{m=-M}^{M} \sum_{q,q'=0}^{Q} c_{m,q} c^*_{m,q'} \xi_{|m|,q,q'}, \tag{43}$$

where P_a and P_r is the active and reactive power, respectively, and the symbol $*$ denotes the operation of conjugation The values of coupling coefficients $\xi_{|m|,q,q'}$ are necessary to calculate constants $c_{m,q}$ from set of equations given by Eq. (D.11) and to obtain the sound power using Eq. (43). There are two equivalent formulas to calculate the coupling coefficients, i.e., the well-known integral formula given by Eq. (D.12) and the proposed formula from Eq. (32). It can be deduced from Eq. (D.12) that the following relation $\xi_{|m|,q,q'} = \xi_{|m|,q',q}$ is satisfied. Therefore, it is enough to find the values of coefficients $\xi_{|m|,q,q'}$ for $q' \le q$.

The sound power is calculated for the frequency range $50 \le f \le 1500$ Hz, assuming that $M = Q = 7$. In Fig. 2 , the active power level $L_a = 10\log_{10}(P_a/P_{ref.})$ and the reactive power level $L_r = 10\log_{10}(P_r/P_{ref.})$, where $P_{ref.} = 1$ pW are presented as the functions of frequency together with the corresponding truncation errors E_t. Different locations of the excited plate's point are investigated. The curves presented in Fig. 2 are obtained based on the values of coupling coefficients calculated from the integral formula given by Eq. (D.12). Figs. 2c and 2d show that the truncation error E_t is less than 1% for almost all the analyzed values of the frequency and for all the considered locations of the excited plate's point. The only exception is the truncation error calculated for the reactive power when $r'_0 = 0.75a$ and $f > 1.35$ kHz. This means that the sound power is calculated for sufficiently large values of the truncation integers M and Q. Assuming the same values for these truncation integers, the sound power is calculated by using the proposed formula from Eq. (32). It should be noted that for a fixed value of the frequency, the relative error E given by Eq. (42) assumes some different values for different coupling coefficients $\xi_{|m|,q,q'}$. Therefore, in this case, the following average error $\overline{E} = \sum_{m=0}^{M} \sum_{q=0}^{Q} \sum_{q'=0}^{q} E_{m,q,q'}$ is analyzed, where $E_{m,q,q'}$ denotes the value of E calculated for the real or imaginary part of the

coupling coefficient $\xi_{|m|,q,q'}$. To show the convergence of the proposed solution, the quantity $\overline{E}$ for the real and imaginary part of $\xi_{|m|,q,q'}$ is presented in Fig. 3 as a function of the truncation integer N for some different values of the truncation integers $M = Q$. Fig. 3 shows that the average error $\overline{E}$ decreases when the value of the truncation integer N increases. This means that the series from Eq. (32) are convergent, and the values of the coupling coefficients can be precisely calculated by using a sufficiently large number of terms in the sums. For example, by performing calculations with $N = 30$, the real and imaginary parts of the coupling coefficients can be calculated with the value of the average relative error $\overline{E}$ smaller than 1%. It can be observed that the values of $\overline{E}$ are greater for the imaginary parts of the coupling coefficients than for the real ones. The value of $\overline{E}$ increases when the number of calculated coupling coefficients increases, i.e., when the values of truncation integers M and Q grow. This indicates that the values of $\xi_{|m|,q,q'}$ are less accurately calculated for higher indices m, q, q'. Here, it should be emphasized that some coefficients with high indices can be inaccurately or even incorrectly calculated. However, great values of the relative errors obtained for some coupling coefficients do not have to lead to a great value of the relative error of the sound power. To explain this fact, the following quantities

$$\Pi^{(a)}_{m,q,q'} = \left|\Re(P_{m,q,q'})\right| / P_a, \qquad \Pi^{(r)}_{m,q,q'} = \left|\Im(P_{m,q,q'})\right| / P_r, \tag{44}$$

can be analyzed, where

$$P_{m,q,q'} = \frac{\pi}{2}\omega^3 a^3 \rho\, \kappa_m \left(c_{m,q} c^*_{m,q'} + c_{-m,q} c^*_{-m,q'}\right) \xi_{|m|,q,q'}, \tag{45}$$

$\Re(u)$ and $\Im(u)$ denote the real part and imaginary part of the complex number u, respectively. The quantities $\Pi^{(a)}_{m,q,q'}$ and $\Pi^{(r)}_{m,q,q'}$ are the normalized contributions from the plate's modes (m, q) and (m, q') to the active and reactive power, respectively. The error of $\xi_{|m|,q,q'}$ produces the error of the quantity $P_{m,q,q'}$. However, it can be concluded that if the values of the quantities $\Pi^{(a)}_{m,q,q'}$ and $\Pi^{(r)}_{m,q,q'}$ are sufficiently small, even a large value of the error obtained for the quantity $P_{m,q,q'}$ cannot generate a large value of the relative error of the sound power. Therefore, the quantity P can be calculated very precisely, which will be shown in the further analysis.

It can be supposed that the sound power can be obtained more efficiently when the coupling coefficients $\xi_{|m|,q,q'}$ are calculated using the formula from Eq. (32) instead of the more time-consuming integral formula given by Eq. (D.12). To prove this hypothesis, the following time ratio t_I/t is investigated, where t_I and t are the times needed to calculate the sound power when the formulas from Eqs. (32) and (D.12) are used, respectively.

The relative error E calculated for the active as well as reactive sound power and the time ratio t_I/t are presented in Fig. 4 as the functions of the truncation integer N for some chosen values of the frequency. Fig. 4 shows that the quantity E decreases when the value of the truncation integers N increases, which proves that the series from Eq. (32) are convergent. Moreover, the time ratio t_I/t decreases when the value of N grows, which is obvious. The relative error E assumes some greater values for the reactive power than for the active one, which can be due to the fact that the imaginary parts of the coupling coefficients $\xi_{|m|,q,q'}$ are calculated with a greater average error $\overline{E}$ than the real parts of these coefficients (see Fig. 3). The value of frequency does not significantly influence the time ratio t_I/t for fixed values of the truncation integers M and Q. It can be concluded that the use of the formula from Eq. (32) provides some accurate results and is much more efficient than the use of the integral formula. For example, the time ratio t_I/t equal to 42 can be achieved with the relative error $E < 0.02\%$ for the active power and $E < 0.13\%$ for the reactive power when $f = 1.2$ kHz and $N = 15$.

The time ratio t_I/t is presented as a function of the truncation integer N in Fig. 5 for some different values of the truncation integers $M = Q$. The relative error E for $M = Q = 4$ and $M = Q = 8$ assumes similar values as in the case presented in Fig. 4 when $M = Q = 6$ and $f = 0.7$ kHz. Therefore, this quantity is not illustrated in Fig. 5. It should be noted that the efficiency of the proposed solution increases when the values of the truncation integers M and Q increase, i.e., when a greater number of plate's modes is used in the calculations. This effect is especially significant when the truncation integer $N < 30$.

To investigate the correctness and numerical efficiency of the proposed formulas for different frequency values, the relative error E for the active and reactive power and the time ratio are presented as a function of frequency in Figs. 6 and 7. Fig. 6 shows that the relative error E and the time ratio t_I/t decrease when the value of the truncation integer N increases. It is worth noting that accurate results can be obtained with a great efficiency by using the presented solution. Making use of the proposed solution for $N = 12$, the sound power can be very efficiently calculated, i.e., at least 48 times quicker than by using the integral formulas. In this case, the relative error does not exceed 1%. The proposed solution can also provide more accurate results. For example, by assuming $N = 27$, the sound power can be calculated with the relative error $E < 0.1\%$ whereas the estimated value of the time ratio is greater than 16.

The time ratio t_I/t is illustrated as a function of the frequency for some different locations of the point excitation (see Fig. 7). The axisymmetric excitation with $r'_0 = 0$ is also investigated. This excitation is the special case for which the truncation integer $M = 0$ and only the coupling coefficients $\xi_{0,q,q'}$ must be calculated. The active and reactive power are calculated with the relative error $E < 1\%$ for all the considered point excitations and for all the analyzed values of frequency. Fig. 7 shows that the sound power can be calculated with the use of the proposed formula from Eq. (32) more than about 16 times quicker than when the integral formula from Eq. (D.12) is employed. This conclusion is true for all the considered excitations, including the symmetric one.

6.2. Efficiency of sound pressure calculations

The solution proposed in this study can also be used to improve sound pressure calculations. In order to investigate the numerical efficiency and correctness of the presented formulas, the sound pressure modulus $|p|$ is calculated with the use of the formulas from Eqs. (9), (10) and (32) as well as by using the known integral formulas given by Eqs. (C.1) and (D.12).

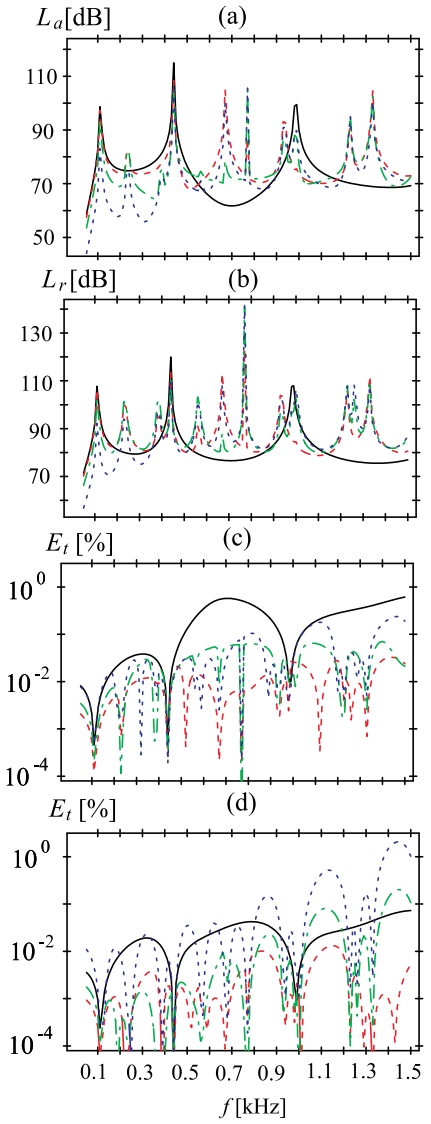

Fig. 2. (a) Active power level L_a, (b) reactive power level L_r, (c) truncation error for the active power P_a and (d) truncation error for the reactive power P_r as the functions of the vibration frequency f for $M = Q = 7$ and the point excitation with different values of the radial coordinate r'_0: solid (black) – $r'_0 = 0$, dashed (red) – $r'_0 = 0.25a$, dashed–dotted (green) – $r'_0 = 0.5a$ and dotted (blue) – $r'_0 = 0.75a$. (For interpretation of the references to color in this figure legend, the reader is referred to the web version of this article.)

The value of the sound pressure level SPL=$20\log_{10}(|p|/p_{ref.})$ is analyzed, where $p_{ref.} = 20$ μPa is the reference value. To validate the proposed solution, the relative error E defined by Eq. (42) is calculated for the sound pressure modulus. The numerical efficiency of the presented formulas is compared with the numerical efficiency of the integral ones by estimating appropriate time ratios.

To prove that the values of the truncation integers M and Q are large enough and the presented results are accurate enough to be considered, the average truncation error $\overline{E_t} = (1/\mathcal{N}) \sum_{j=1}^{\mathcal{N}} E_t^{(j)}$ is investigated, where $E_t^{(j)}$ is the value of the truncation error from Eq. (41) calculated for a jth curve's point and $\mathcal{N}$ is the number of the curve's points. The values of $\overline{E_t}$ are presented in the figures' captions. It should be noted that $\overline{E_t} < 0.3\%$ for all the analyzed cases except the one curve for which the truncation error $\overline{E_t} < 1.3\%$ (see Fig. 12). This means that the values of the truncation integers M and Q are correctly chosen.

The proposed formulas are tested by obtaining the frequency responses for the sound pressure modulus at fixed field points. In Fig. 8, SPL, the relative error E and the time ratio t_I/t are presented as the functions of the frequency, where t_I and t are the times needed to calculate the coupling coefficient $\xi_{|m|,q,q'}$, to find the constants $c_{m,q}$ from the set of equations given by Eq. (D.11) and to calculate the value of the sound pressure modulus at the considered field point. The time t_I is the time needed to perform calculations with the use of the integral formulas from Eqs. (C.1) and (D.12), and the time t was estimated for calculations performed by using the formulas given by Eqs. (32), (9), (10), (13), (23) and (28). Fig. 8 shows that the proposed solution can be used to accurately

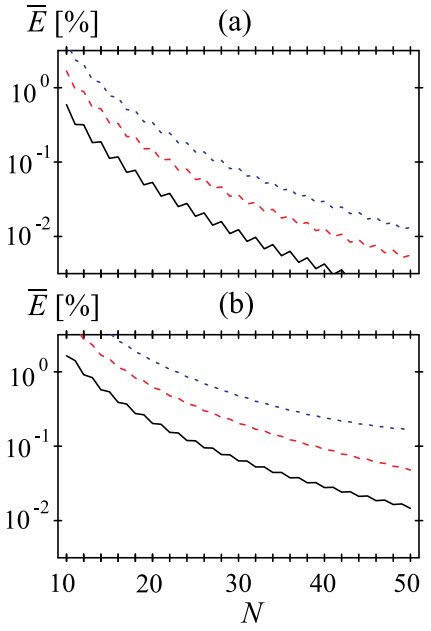

Fig. 3. (a) Average relative error $\overline{E}$ calculated for the real part of the coupling coefficients $\xi_{|m|,q,q'}$, (b) average relative error $\overline{E}$ calculated for the imaginary part of $\xi_{|m|,q,q'}$ as the functions of the truncation integer N for $f = 0.7$ kHz. Lines keys: solid (black) – $M = Q = 4$, dashed (red) – $M = Q = 6$ and dotted (blue) $M = Q = 8$. (For interpretation of the references to color in this figure legend, the reader is referred to the web version of this article.)

and efficiently calculate the sound pressure modulus at any field point and for an arbitrary value of frequency. The relative error is less than 0.1% for all the cases, except for some narrow frequency ranges, and the time ratio t_I/t assumes values greater than about 9. The sound pressure modulus can be calculated at the field point $(10a, \pi/4, \pi/2)$ more than 12 times quicker by using the proposed formulas than with the use of the integral ones when $f > 650$ Hz. The local maximum of the time ratio can be observed when the value of frequency is equal to about 500 Hz. However, this effect is difficult to explain because it is probably caused by built-in algorithms for numerical integrations. Taking into account that $J_m(0) = 0$ for $m > 0$, it can be concluded from Eq. (C.2) that the use of the formula given by Eq. (C.1) is the most efficient when $\theta = 0$ and the time t_I assumes in this case the smallest value. This fact can explain the greater value of the time ratio t_I/t obtained for $\theta = \pi/4$ than for $\theta = 0$ (see Fig. 8c curves red and blue). The time ratio t_I/t is greater for $r = 3a$ than for $r = 0.5a$ (see curves red and black). This behavior of the quantity t_I/t is obvious and is due to the different number of terms in the formulas from Eqs. (9) and (10).

To prove that the proposed solution is convergent and its accuracy increases when the value of the truncation integer N grows, the sound pressure modulus at the chosen field point is presented in Fig. 9 as a function of the frequency for some different values of N. Fig. 9 clearly shows that the relative error E decreases when the value of N increases. Moreover, it can be observed that the value of frequency does not significantly influence the time ratio t_I/t. This quantity is greater than 3.9, even when the accuracy of the results obtained for $N = 40$ is very high. Hence, it can be concluded that the presented solution is convergent and useful for accurate calculations of the sound pressure. The sound pressure modulus can be calculated with the relative error $E < 1\%$ and more than 20 times quicker by using the proposed solution with $N = 18$ than by employing the integral formulas. Moreover, making use of the presented formulas with $N = 8$, the quantity $|p|$ can be accurately and efficiently calculated with $E < 0.1\%$ and time ratio $t_I/t > 49$ when $f < 0.3$ kHz.

The usefulness of the proposed solution for obtaining the sound pressure distribution is investigated for a fixed value of frequency. The efficiency of the presented formulas is compared with the efficiency of the integral formulas for the two different calculation strategies. The first strategy is to obtain the distribution of $|p|$ in the case when only the coefficients listed in the hints 1 and 2 in Section 5 are stored in a computer's memory. The calculations are performed using the integral formulas in the time t_I. For this purpose, the coupling coefficients $\xi_{|m|,q,q'}$ are calculated based on Eq. (D.12), the constants $c_{m,q}$ are found from the set of equations given by Eq. (D.11) and the values of $|p|$ at the considered field points are calculated by using Eq. (C.1). The distribution of $|p|$ is also obtained using the presented solution in the time t needed to calculate the coupling coefficient $\xi_{|m|,q,q'}$ based on Eq. (32), to find constants $c_{m,q}$ from the set of equations given by Eq. (D.11), to obtain the constants $\vartheta_{m,l,n}$, $A_{m,n}$ and $B_{m,l}$ and to calculate the values of $|p|$ at the considered field points by using Eqs. (9) and (10). In the case of the second strategy, it is assumed that the values of the constants $c_{m,q}$, $\vartheta_{m,l,n}$, $A_{m,n}$ and $B_{m,l}$ were calculated and stored in the computer's memory. The values of the sound pressure modulus are calculated based on the integral formula given by Eq. (C.1) in the time $t_I^{(cur.)}$ and using the formulas from Eqs. (9) and (10) in the time $t^{(cur.)}$. The values of the time ratios t_I/t and $t_I^{(cur.)}/t^{(cur.)}$ describing the numerical efficiency of the presented solution for both strategies are presented in the captions of Figs. 10 and 11.

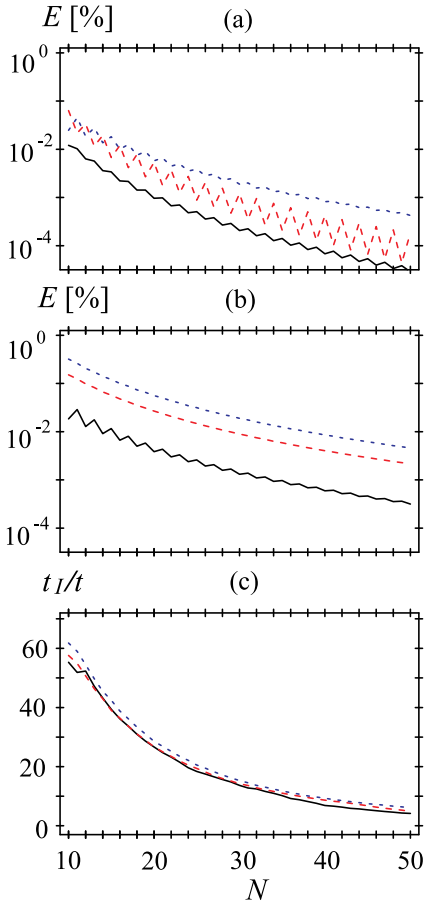

Fig. 4. (a) Relative error E for the active sound power P_a, (b) relative error E for the reactive sound power P_r and (c) time ratio t_I/t as the functions of the truncation integer N for $M = Q = 6$ and the point excitation of the radial coordinate $r_0' = 0.5a$. Lines keys: solid (black) – $f = 0.2$ kHz, dashed (red) – $f = 0.7$ kHz and dotted (blue) $f = 1.2$ kHz. (For interpretation of the references to color in this figure legend, the reader is referred to the web version of this article.)

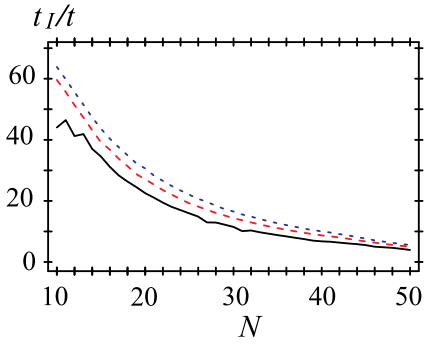

Fig. 5. Time ratio t_I/t for the sound power as a function of the truncation integer N for $f = 0.7$ kHz, the point excitation of the radial coordinate $r_0' = 0.5a$ and: black – $M = Q = 4$, red – $M = Q = 6$ and blue – $M = Q = 8$. (For interpretation of the references to color in this figure legend, the reader is referred to the web version of this article.)

The sound pressure level calculated based on the proposed solution and the relative error E are presented in Fig. 10 as the functions of the coordinate θ for symmetric and asymmetric point excitation and at some chosen field point located inside the subregions 1 and 2. It should be noted that the integrand in Eq. (C.2) contains the expression $\exp(-\sqrt{\tau^2 - k^2}z)$ for $\tau > k$ which means that it is the most slowly convergent when $z = 0$. Hence, some numerical errors due to some troublesome numerical integrations can occur when the value of θ approaches $\pi/2$. This effect is demonstrated by the rapid increase in the value of the relative error E when θ approaches $\pi/2$. It can be emphasized that the integral formulas cannot be used to obtain the accurate value of the sound

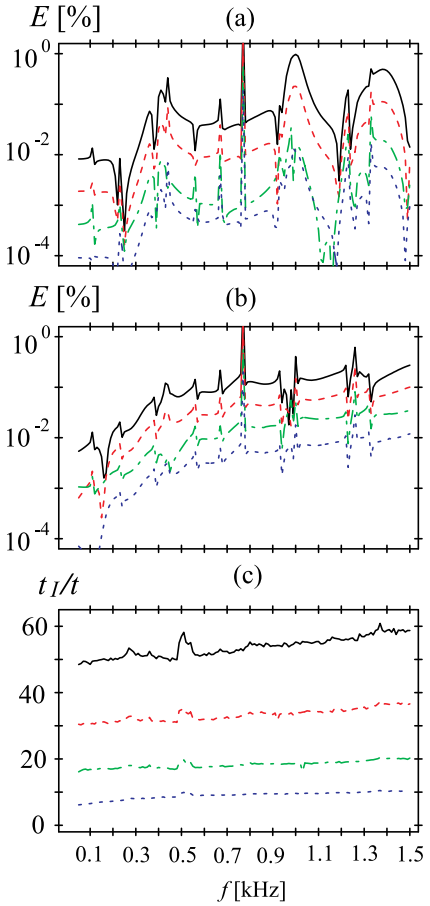

Fig. 6. (a) Relative error E for the active power P_a, (b) relative error E for the reactive power P_r and (c) time ratio t_I/t for the sound power as the functions of the frequency f for $M = Q = 7$ and the point excitation of the radial coordinate $r'_0 = 0.5a$. Line keys: solid (black) – $N = 12$, dashed (red) – $N = 18$, dashed–dotted (green) – $N = 27$ and dotted (blue) – $N = 40$. (For interpretation of the references to color in this figure legend, the reader is referred to the web version of this article.)

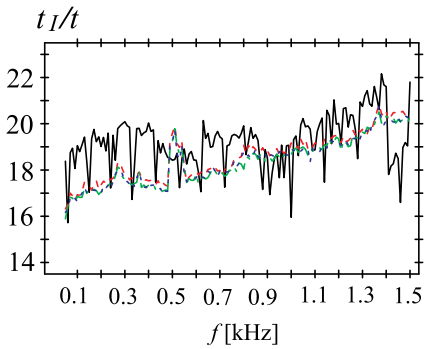

Fig. 7. Time ratio t_I/t for the sound power as a function of the frequency f for $N = 27$, $Q = 7$ and the point excitation with different values of the radial coordinate r'_0. Line keys: solid (black) – $r'_0 = 0$ and $M = 0$, dashed (red) – $r'_0 = 0.25a$ and $M = 7$, dashed–dotted (green) – $r'_0 = 0.5a$ and $M = 7$ and dotted (blue) – $r'_0 = 0.75a$ and $M = 7$. (For interpretation of the references to color in this figure legend, the reader is referred to the web version of this article.)

pressure in this special case, and the only method is the use of the proposed solution. However, except for the field points with a value of θ close to $\pi/2$, the value of the relative error E is less than about 0.1% which means that the results obtained by using the proposed solution agree with those given by the integral formulas. The values of the time ratios presented in the caption of Fig. 10 prove that the use of the proposed solution can significantly improve the numerical calculations for both numerical strategies and for any value of the coordinate r. The numerical efficiency was investigated in the symmetric and asymmetric cases. For the subregion

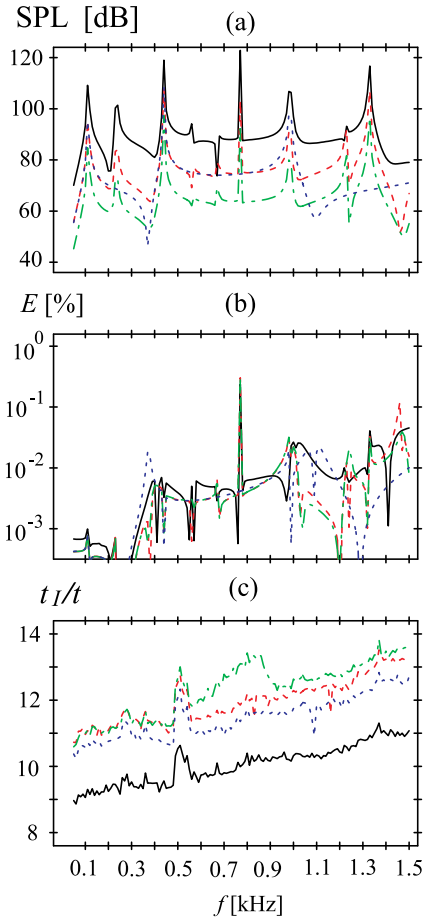

Fig. 8. (a) SPL, (b) relative error E and (c) time ratio t_I/t for the sound pressure modulus $|p|$ as the functions of the frequency f for $N = 27$, $M = Q = 7$, $\varphi = \pi/2$ and the point excitation with the polar coordinates $r_0' = 0.5a$ and $\varphi_0 = \pi/4$. Line keys: solid (black) – $r = 0.5a$, $\theta = \pi/4$ ($\overline{E_t} = 0.03\%$), dashed (red) – $r = 3a$, $\theta = \pi/4$ ($\overline{E_t} = 0.03\%$), dashed–dotted (green) – $r = 10a$, $\theta = \pi/4$ ($\overline{E_t} = 0.03\%$), dotted (blue) – $r = 3a$, $\theta = 0$ ($\overline{E_t} = 0.10\%$). (For interpretation of the references to color in this figure legend, the reader is referred to the web version of this article.)

1, when the formula from Eq. (9) with the greater number of terms has to be used, the time ratios assume the great values $t_I/t = 30$ and $t_I^{(cur.)}/t^{(cur.)} = 60$ for the asymmetric point excitation and $t_I/t = 26$ and $t_I^{(cur.)}/t^{(cur.)} = 33$ for the symmetric one. If $r = 10a$ and the second numerical strategy is realized, the considered sound pressure distribution can be obtained 207 times quicker by using the proposed solution than by employing the integral formulas. The time ratios also assume great values for the subregion 2 and the symmetric case.

It is of interest to investigate the applicability of the proposed solution for calculating the acoustic field at resonance frequencies. For this purpose, the sound pressure level and the relative error E were presented in Fig. 11 as the functions of the normalized coordinate r/a. The axial distribution of the sound pressure modulus was illustrated, i.e., when $\theta = 0$. The plate's resonance frequencies were calculated from the following formula $f_{m,q}^{(res.)} = 1/(2\pi)(g_{|m|,q}/a)^2\sqrt{D_E/(\rho_p h)}$, where $f_{m,q}^{(res.)}$ is the resonance frequency related to the plate's mode (m, q) [32]. The acoustic field was analyzed for the four lowest resonance frequencies associated with the plate's modes $(0, 0)$, $(1, 0)$, $(2, 0)$ and $(0, 1)$, respectively.

Fig. 11 shows that, for $r > a$, the sound pressure level decreases when the value of the coordinate r increases. This behavior of the acoustic pressure is expected. Moreover, the local extremum of SPL can be observed for the third and fourth resonance frequency when $r < a$.

It can be observed that the relative error increases when the value of the coordinate r approaches zero. As already mentioned, this behavior of the relative error is due to a slow convergence of the integrand from Eq. (C.2). However, Fig. 11 proves that the proposed solution can be used to obtain accurate results at resonance frequencies. For example, the quantity E does not exceed the value of 0.05% for the frequency $f = f_{1,0}^{(res.)} = 235.4$ Hz with the exception of the cases when the value of the coordinate r is close to zero. Moreover, the relative error is less than 1.25% for all the analyzed field points when $f = f_{2,0}^{(res.)} = 386.1$ Hz. The increase in the value of the coordinate r does not influence the value of E when $r > 2a$. This means that the presented formulas are also accurate in the far field. Moreover, Fig. 11 shows that, for $r > a$, the relative error E increases when the value of the resonance frequency increases.

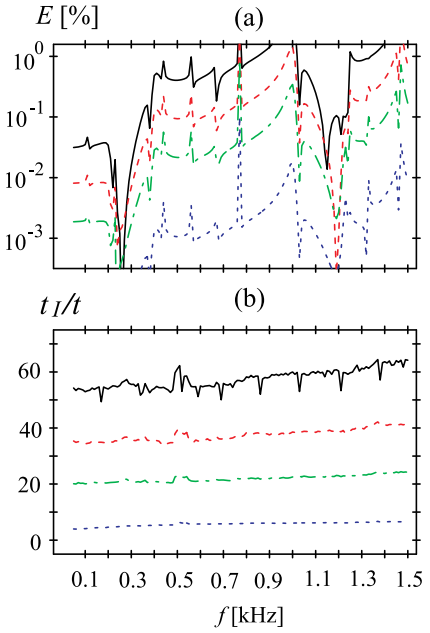

Fig. 9. (a) Relative error E and (b) time ratio t_I/t for the sound pressure modulus $|p|$ as the functions of the frequency f for $M = Q = 7$, $r = 3a$, $\theta = \pi/4$, $\varphi = \pi/2$ and the point excitation with the polar coordinates $r_0' = 0.5a$ and $\varphi_0 = \pi/4$. Line keys: solid (black) – $N = 8$, dashed (red) – $N = 12$, dashed–dotted (green) – $N = 18$ and dotted (blue) – $N = 40$. (For interpretation of the references to color in this figure legend, the reader is referred to the web version of this article.)

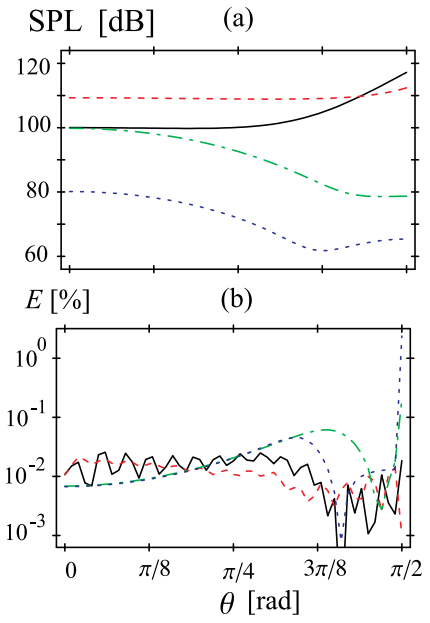

Fig. 10. (a) SPL, (b) relative error E as the functions of the coordinate θ for $f = 1$ kHz, $Q = 6$, $N = 27$, $\varphi = 0$ and the point excitation with different values of the polar coordinates r_0' and φ_0. Line keys: black – $M = 6$, $r_0' = 0.75a$, $\varphi_0 = 5\pi/4$, $r = 0.5a$ ($t_I/t = 30$, $t_I^{(cur.)}/t^{(cur.)} = 60$, $\overline{E_t} = 0.02\%$), red – $M = 0$, $r_0' = 0$, $r = 0.5a$ ($t_I/t = 26$, $t_I^{(cur.)}/t^{(cur.)} = 33$, $\overline{E_t} = 0.03\%$), green – $M = 0$, $r_0' = 0$, $r = 3a$ ($t_I/t = 56$, $t_I^{(cur.)}/t^{(cur.)} = 225$, $\overline{E_t} = 0.02\%$), blue – $M = 6$, $r_0' = 0.75a$, $\varphi_0 = 5\pi/4$, $r = 10a$ ($t_I/t = 54$, $t_I^{(cur.)}/t^{(cur.)} = 207$, $\overline{E_t} = 0.04\%$). (For interpretation of the references to color in this figure legend, the reader is referred to the web version of this article.)

Taking into account that all the values of the time ratios t_I/t and $t_I^{(cur.)}/t^{(cur.)}$ estimated at the resonance frequencies are greater than 25, it can be concluded that the use of the proposed numerical technique is much more efficient than the use of the integral formulas.

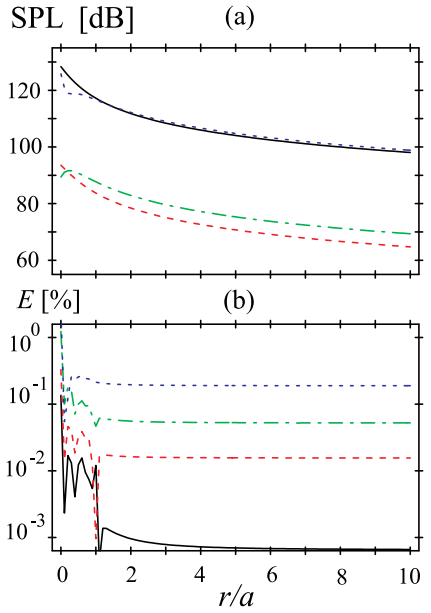

Fig. 11. (a) SPL, (b) relative error E as the functions of the normalized coordinate r/a for $M = Q = 5$, $N = 12$, $\theta = 0$, $\varphi = 0$ and the point excitation with the polar coordinates $r_0' = 0.25a$ and $\varphi_0 = \pi/4$. Line keys: solid (black) – $f = f_{0,0}^{(res.)} = 113.1$ Hz ($t_I/t = 27$, $t_I^{(cur.)}/t^{(cur.)} = 26$, $\overline{E_t} = 0.1 \cdot 10^{-4}\%$), dashed (red) – $f = f_{1,0}^{(res.)} = 235.4$ Hz ($t_I/t = 29$, $t_I^{(cur.)}/t^{(cur.)} = 27$, $\overline{E_t} = 22.2 \cdot 10^{-4}\%$), dashed–dotted (green) – $f = f_{2,0}^{(res.)} = 386.1$ Hz ($t_I/t = 29$, $t_I^{(cur.)}/t^{(cur.)} = 27$, $\overline{E_t} = 36.2 \cdot 10^{-4}\%$) dotted (blue) – $f = f_{0,1}^{(res.)} = 440.3$ Hz ($t_I/t = 29$, $t_I^{(cur.)}/t^{(cur.)} = 28$, $\overline{E_t} = 0.4 \cdot 10^{-4}\%$). (For interpretation of the references to color in this figure legend, the reader is referred to the web version of this article.)

From a practical point of view, it is interesting to determine the sound field when the value of the frequency is close to the critical frequency of the plate. This critical frequency f_c is given by the following formula $f_c = c^2/(2\pi)\sqrt{\rho_p h/D_E}$ and is equal to 11963.1 Hz for the considered plate [33]. In order to prove that the proposed method can be used in the case when the value of frequency is near the critical frequency of the plate, the sound pressure level and the relative error E were presented in Fig. 12 as the functions of the normalized coordinate r/a for $f = 11.963$ kHz. In the case of $\theta = \pi/8$ and $\theta = 3\pi/8$, the quantity $E < 0.5\%$ for all the analyzed values of the coordinate r. The increase in the value of the coordinate r does not lead to an increase in the relative error when $r > 6a$ and $\theta = \pi/8$ as well as when $r > 3a$ and $\theta = 3\pi/8$. For $\theta = \pi/4$ and $r > 2a$, the quantity E increases when the value of the coordinate r increases. However, the relative error for all the analyzed values of the coordinate r does not exceed the value of 1.2% when $\theta = \pi/4$. The time ratios assume great values for all the analyzed cases. For example, using the proposed solution instead of the integral formulas, the sound field distribution can be obtained about 26 times quicker for the first strategy and 37 times quicker for the second one when $\theta = 3\pi/8$.

Fig. 12 proved that using the presented numerical technique, the acoustic field can be calculated when the frequency value is close to the critical frequency of the plate. Furthermore, since the critical frequency assumes a high value, the proposed approach can also accurately calculate the acoustic pressure at high frequencies.

The results of the numerical analysis presented in this section show that the proposed solution gives accurate results, and its numerical efficiency is much greater than the numerical efficiency of the integral solution. With the special scripts provided upon reasonable request, the readers can perform numerical simulations using their hardware and software. These scripts enable the readers to test the accuracy of the proposed solution and estimate the time ratios.

7. Conclusions

By dividing the half-space into the two subregions and coupling them with the use of the continuity conditions, the numerically efficient solution is obtained to calculate the sound power and the sound pressure radiated by any circular sound source located in a flat, infinite and perfectly rigid baffle. The considered sound source can be, for example, a membrane, a plate with an arbitrary boundary condition, as well as an input of a circular waveguide or cavity. The accuracy and numerical efficiency of the proposed method were tested in the case where the sound source is a clamped circular plate. In order to compare the results obtained by using the presented formulas with those given by the known integral solution, the relative error was analyzed. The value obtained from the integral formulas was considered as exact. The numerical efficiency of the proposed method was compared with the numerical efficiency of the integral formulas. For this purpose, the times needed to calculate the value of the considered physical quantity with the use of the presented solution as well as the integral one were estimated, and then their ratio was analyzed.

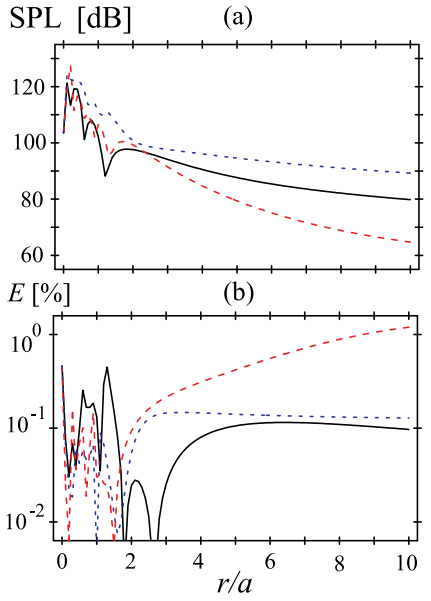

Fig. 12. (a) SPL, (b) relative error E as the functions of the normalized coordinate r/a for $f = 11.963$ kHz, $M = Q = 10$, $N = 50$, $\varphi = \pi$ and the point excitation with the polar coordinates $r_0' = 0.25a$ and $\varphi_0 = \pi/4$. Line keys: solid (black) – $\theta = \pi/8$ ($t_I/t = 26$, $t_I^{(cur.)}/t^{(cur.)} = 36$, $\overline{E_t} = 0.25\%$), dashed (red) – $\theta = \pi/4$ ($t_I/t = 27$, $t_I^{(cur.)}/t^{(cur.)} = 38$, $\overline{E_t} = 1.28\%$), dotted (blue) – $\theta = 3\pi/8$ ($t_I/t = 26$, $t_I^{(cur.)}/t^{(cur.)} = 37$, $\overline{E_t} = 0.25\%$). (For interpretation of the references to color in this figure legend, the reader is referred to the web version of this article.)

The numerical analysis clearly shows that the proposed method can be used to improve the calculations of the sound power as well as the sound pressure. The detailed conclusions can be formulated as follows:

- Using the presented formulas, the coupling coefficients can be efficiently and accurately calculated, which improves the sound power calculations. For example, by using the obtained formulas instead of the integral ones, the calculations of the sound power can be performed more than 48 times quicker, and the value of the relative error is less than 1%. Moreover, the numerical analysis shows that the improvement in obtaining the sound power is more significant when a greater number of the plate's modes is used in calculations.
- The proposed solution can be used to efficiently obtain accurate values of the sound pressure modulus at all the field points, even for the value of the inclination angle close to $\pi/2$, i.e., in the case when the integral formulas can fail. Hence, it can be stated that the use of the presented formulas is the only method to accurately calculate the sound pressure.
- The proposed method can improve the sound pressure calculations at a fixed field point and for a changing frequency value, i.e., when the coupling coefficients have to be calculated each time. Making use of the presented formulas instead of the integral ones, the numerical calculations can be performed more than 9 times quicker, and the relative error value is less than 0.1%.
- The distribution of the sound pressure can also be obtained more efficiently by using the presented formulas. For this purpose, the calculated values of some coefficients and constants can be stored in the computer's memory. The sound pressure distribution can be obtained even more than 200 times quicker and with a relative error value less than 0.1% using the presented formulas than employing the integral ones. The presented formulas are less efficient when the radial distance of the field point is less than the plate's radius. However, even in this case, the sound pressure distribution can be obtained 60 times quicker.
- The proposed formulas can be used to efficiently and accurately calculate the sound pressure modulus at the plate's resonant frequencies, as well as at high frequencies close to the plate's critical frequency.

CRediT authorship contribution statement

Krzysztof Szemela: Writing – original draft, Visualization, Software, Methodology, Formal analysis, Conceptualization. **Wojciech P. Rdzanek:** Writing – review & editing, Methodology, Formal analysis, Conceptualization. **Marek Pawelczyk:** Writing – review & editing, Methodology, Conceptualization. **Li Cheng:** Writing – review & editing, Methodology, Conceptualization.

Declaration of competing interest

The authors declare that they have no known competing financial interests or personal relationships that could have appeared to influence the work reported in this paper.

Data availability

Data will be made available on request.

Acknowledgments

The research presented in this paper was partially supported by the Center for Innovation and Transfer of Natural Sciences and Engineering Knowledge Project at The University of Rzeszów, Poland.

The work was supported in part by the project IN-NOVA: "Active reduction of noise transmitted into and from enclosures through encapsulated structures", which has received funding from the European Union's Horizon Europe program under the Marie Sklodowska-Curie grant agreement no. 101073037.

Appendix A. Rigorous formulas for coefficients $X_{\nu,n}$

Making use of the following definition $j_\nu(w) = \sqrt{\pi/(2w)}J_{\nu+1/2}(w)$, the coefficients from Eq. (21) can be written as

$$X_{\nu,n} = \frac{\pi}{2\sqrt{\gamma_{\nu,n}}}\int_0^1 J_{\nu+1/2}(w)J_{\nu+1/2}(\gamma_{\nu,n}w)wdw, \tag{A.1}$$

where $J_\nu(\cdot)$ is the Bessel function of the ν-th order. Then, using the well-known formula for the integration of the product of the Bessel functions results in

$$X_{\nu,n} = \frac{\pi}{2\sqrt{\gamma_{\nu,n}}(1-\gamma_{\nu,n}^2)}[J_{\nu+3/2}(1)J_{\nu+1/2}(\gamma_{\nu,n}) - \gamma_{\nu,n}J_{\nu+3/2}(\gamma_{\nu,n})J_{\nu+1/2}(1)]. \tag{A.2}$$

The formula from Eq. (A.2) cannot be used when $\nu = n = 0$ which is due to the fact that $\gamma_{0,0} = 0$. This special case must be considered separately. Taking into account that $j_0(w) = \sin(w)/w$, the coefficient $X_{0,0}$ can be expressed as

$$X_{0,0} = \int_0^1 \sin(w)wdw = \sin(1) - \cos(1). \tag{A.3}$$

Appendix B. Rigorous formulas for coefficients $Y_{|m|,l}$

By using substitution $w = \cos\theta$, the integral from Eq. (18) can be transformed into the following form

$$Y_{|m|,l} = \int_0^1 P_{|m|+1}^{|m|}(w)P_{|m|+2l}^{|m|}(w)dw. \tag{B.1}$$

The associated Legendre polynomials can be expressed as

$$P_l^{|m|}(w) = \frac{(-1)^{|m|}}{2^l l!}(1-w^2)^{|m|/2}\Theta_{l+|m|}^{(l)}(w), \tag{B.2}$$

where $\Theta_n^{(\nu)}(w) = d^n\left[(w^2-1)^\nu\right]/dw^n$ and the following relation

$$P_l^{-|m|}(w) = (-1)^m\frac{(l-|m|)!}{(l+|m|)!}P_l^{|m|}(w), \tag{B.3}$$

is satisfied [31]. In the light of Eqs. (B.2) and (B.3), the associated Legendre polynomials can also be defined as

$$P_l^{|m|}(w) = \frac{(l+|m|)!}{(l-|m|)!2^l l!}(1-w^2)^{-|m|/2}\Theta_{l-|m|}^{(l)}(w). \tag{B.4}$$

By expressing the functions $P_{|m|+1}^{|m|}(w)$ and $P_{|m|+2l}^{|m|}(w)$ with the use of Eqs. (B.2) and (B.4), respectively, and taking into account that $\Theta_{2|m|+1}^{(|m|+1)}(w) = (2|m|+2)!w$, the coefficients $Y_{|m|,l}$ can be written as

$$Y_{|m|,l} = \frac{(-1)^{|m|}(2|m|+2l)!(2|m|+2)!}{2^{2|m|+2l+1}(|m|+1)!(2l)!(|m|+2l)!}\int_0^1 w\Theta_{2l}^{(|m|+2l)}(w)dw. \tag{B.5}$$

In the special case when $l = 0$, the coefficients from Eq. (B.1) can be calculated as follows

$$Y_{|m|,0} = \frac{(-1)^{|m|}(2|m|)!(2|m|+2)!}{2^{2|m|+1}(|m|+1)!|m|!}\int_0^1(w^2-1)^{|m|}wdw = \frac{(2|m|)!(2|m|+2)!}{4^{|m|+1}[(|m|+1)!]^2} \quad \text{for} \quad l = 0. \tag{B.6}$$

By using integration by parts, and taking into account that $\Theta_n^{(\nu)}(1) = 0$ if $\nu > n$, Eq. (B.5) for $l > 0$ can be formulated as

$$Y_{|m|,l} = \frac{(-1)^{|m|}(2|m|+2l)!(2|m|+2)!}{2^{2|m|+2l+1}(|m|+1)!(2l)!(|m|+2l)!}\Theta_{2l-2}^{(|m|+2l)}(0). \tag{B.7}$$

Now, it is necessary to calculate the following expression $\Theta_n^{(\nu)}(0)$ for $\nu > n$ and an even value of n. For this purpose, the Newton's binomial theorem is used to obtain the following formula

$$\Theta_n^{(\nu)}(w) = \sum_{j=0}^{\nu} \frac{\nu!}{j!(\nu-j)!} \frac{d^n w^{2\nu}}{dx^n} (-1)^{\nu-j}. \tag{B.8}$$

When $w = 0$ and n is an even number, it can be deduced that only the term with the index $j = n/2$ is not equal to zero. Hence, the following formula can be written

$$\Theta_n^{(\nu)}(0) = \frac{\nu! n! (-1)^{\nu-n/2}}{(n/2)!(\nu-n/2)!}. \tag{B.9}$$

Finally, combining Eqs. (B.7) and (B.9) results in

$$Y_{|m|,l} = \frac{-(-1)^l (2|m|+2l)!(2|m|+2)!}{4^{|m|+l+1}(|m|+1)!\, l!\, (|m|+l+1)!(2l-1)}. \tag{B.10}$$

It should be noted that Eq. (B.10) for $l = 0$ is equivalent to Eq. (B.6) which is valid only for $l = 0$. This means that the formula given by Eq. (B.10) can be used for $l \geq 0$.

Appendix C. Integral formula for an acoustic pressure radiated by a baffled circular source

Making use of the Hankel transform, the basic problem of sound radiation by a circular sound source located in a perfectly rigid infinite baffle defined by Eqs. (1)–(4) was analytically solved. The sound pressure distribution in the cylindrical coordinate system (r', φ, z) was presented as [28]

$$p(r', \varphi, z) = -i\omega^2 \rho a^2 \sum_{m=-M}^{M} \sum_{q=0}^{Q} c_{m,q} p_{|m|,q}(r', z) e^{im\varphi}, \tag{C.1}$$

where

$$p_{|m|,q}(r', z) = \int_0^{\infty} \frac{\Phi_{|m|,q}(\tau)}{\mu} J_{|m|}(\tau r') e^{i\mu z} \tau d\tau, \tag{C.2}$$

$$\Phi_{|m|,q}(\tau) = \frac{1}{a^2} \int_0^a W_{|m|,q}(r') J_{|m|}(\tau r') r' dr', \tag{C.3}$$

$c_{m,q}$ are constants that can be found by solving the equation of motion of a considered sound source, and $\mu = \sqrt{k^2 - \tau^2}$ for $\tau < k$ and $\mu = i\sqrt{\tau^2 - k^2}$ for $\tau > k$.

In the special case when the sound source is a clamped circular plate of the radius a, the eigenfunctions $W_{|m|,q}(r')$ can be written as [28,32,34]

$$W_{|m|,q}(r') = U_{|m|,q} \left[J_{|m|}(g_{|m|,q} r'/a) - \frac{J_{|m|}(g_{|m|,q})}{I_{|m|}(g_{|m|,q})} I_{|m|}(g_{|m|,q} r'/a) \right], \tag{C.4}$$

where $U_{|m|,q} = 1/\left[\sqrt{2} J_{|m|}(g_{|m|,q})\right]$ and $g_{|m|,q}$ are the eigenvalues calculated from the following eigenequation

$$J_{|m|}(g_{|m|,q}) I_{|m|+1}(g_{|m|,q}) + J_{|m|+1}(g_{|m|,q}) I_{|m|}(g_{|m|,q}) = 0. \tag{C.5}$$

The function $\Phi_{|m|,q}(\tau)$ for the clamped circular plate can be expressed as

$$\Phi_{|m|,q}(\tau) = \frac{2U_{|m|,q} g_{|m|,q}^2}{g_{|m|,q}^4 - (\tau a)^4} \left[g_{|m|,q} J_{|m|}(\tau a) J_{|m|+1}(g_{|m|,q}) - \tau a J_{|m|}(g_{|m|,q}) J_{|m|+1}(\tau a) \right]. \tag{C.6}$$

The equation of motion for the clamped circular plate, necessary for calculating constants $c_{m,q}$, is presented in Appendix C. After calculating unknown constants, the acoustic pressure distribution can be found from Eq. (C.1). Here, it should be emphasized that this formula contains the series of improper integrals calculated from zero to infinity. This means that the sound pressure calculations with the use of this formula can be troublesome and time-consuming. Moreover, some numerical errors produced by procedures of numerical integration can lead to inaccurate or even incorrect values of sound pressure.

Appendix D. Solution of the equation of motion for a clamped circular plate

Forced vibrations of a circular plate can be described by the following equation (cf. [28])

$$\left(k_D^{-4} \nabla^4 - 1\right) W(r', \varphi) + \frac{p_s(r', \varphi)}{\rho_p h \omega^2} = \frac{f(r', \varphi)}{\rho_p h \omega^2}, \tag{D.1}$$

where $k_D = \sqrt[4]{\omega^2 \rho_p h / D}$ is the bending wavenumber, ρ_p and h denote the plate's density and its thickness, respectively, $D = D_E(1+i\eta)$ is the complex bending stiffness, $D_E = Eh^3/[12(1-\nu^2)]$ is the bending stiffness, E and ν are the plate's Young modulus and the Poisson ratio, respectively, η is the damping coefficient, $f(r', \varphi)$ is the external excitation, and $p_s(r', \varphi)$ is the pressure produced by the fluid acting on the upper plate's surface. It was assumed that the lower plate's surface is not loaded by the fluid.

The solution of the equation of motion can be expressed as [32,34]

$$W(r', \varphi) = \sum_{m=-M}^{M} \sum_{q=0}^{Q} c_{m,q} \tilde{W}_{m,q}(r', \varphi), \tag{D.2}$$

where $\tilde{W}_{m,q}(r', \varphi) = W_{|m|,q}(r') e^{im\varphi}$ are the normalized plate's eigenfunctions, $W_{|m|,q}(r')$ are the radial parts of the eigenfunctions, $c_{m,q}$ are constants to find and M and Q are the truncation integers, which will be determined so that the obtained results can be accurate enough. The eigenfunctions satisfy the following orthogonality relation

$$\int_{S_p} \tilde{W}_{m,q}(r', \varphi) \tilde{W}^*_{m,q}(r', \varphi) dS_p = S \delta_{m,m'} \delta_{q,q'}, \tag{D.3}$$

where S_p is the plate's surface, the symbol $*$ denotes the operation of conjugation, $S = \pi a^2$ is the plate's area, and $\delta_{m,m'}$ is the Kronecker delta. Moreover, the following equation [32,34]

$$\nabla^4 \tilde{W}_{m,q}(r', \varphi) = k^4_{|m|,q} \tilde{W}_{m,q}(r', \varphi), \tag{D.4}$$

where $k_{|m|,q} = g_{|m|,q}/a$ denotes the modal wavenumber, is true.

Inserting the solution from Eq. (D.2) into the equation of motion given by Eq. (D.1), and then using Eq. (D.4) and the orthogonality of the plate's eigenfunctions, the following set of equations can be obtained

$$c_{m,q} \left(\frac{k^4_{|m|,q}}{k^4_D} - 1 \right) + \frac{P_{m,q}}{\rho_p h \omega^2 S} = \frac{F_{m,q}}{\rho_p h \omega^2 S}, \tag{D.5}$$

$m = -M, \ldots, M$, $q = 0, \ldots, Q$, where

$$P_{m,q} = \int_{S_p} p_s(r', \varphi) \tilde{W}^*_{m,q}(r', \varphi) dS_p, \tag{D.6}$$

$$F_{m,q} = \int_{S_p} f(r', \varphi) \tilde{W}^*_{m,q}(r', \varphi) dS_p. \tag{D.7}$$

The pressure distribution on the plate's surface can be expressed as

$$p_s(r', \varphi) = \sum_{m=-M}^{M} \sum_{q=0}^{Q} c_{m,q} p^{(r)}_{|m|,q}(r') e^{im\varphi}, \tag{D.8}$$

where $p^{(r)}_{|m|,q}(r')$ are known functions.

In the light of Eq. (D.8), the factor from Eq. (D.6) takes the form

$$P_{m,q} = -i\omega^2 \rho a S \sum_{q'=0}^{Q} c_{m,q'} \xi_{|m|,q,q'}, \tag{D.9}$$

where

$$\xi_{|m|,q,q'} = \frac{2i}{\omega^2 \rho a^3} \int_0^a p^{(r)}_{|m|,q'}(r') W_{|m|,q}(r') r' dr', \tag{D.10}$$

are the coupling coefficients.

Inserting Eq. (D.10) into Eq. (D.5) leads to

$$c_{m,q} \left(\frac{k^4_{|m|,q}}{k^4_D} - 1 \right) - i \frac{\rho a}{\rho_p h} \sum_{q'=0}^{Q} c_{m,q'} \xi_{|m|,q,q'} = \frac{F_{m,q}}{\rho_p h \omega^2 S}. \tag{D.11}$$

Taking into account that $p^{(r)}_{|m|,q'}(r') = p_{|m|,q'}(r', 0)$ and using Eq. (C.3), the coupling coefficients can be written as

$$\xi_{|m|,q,q'} = 2a \int_0^\infty \frac{\boldsymbol{\Phi}_{|m|,q}(\tau) \boldsymbol{\Phi}_{|m|,q'}(\tau)}{\mu} \tau d\tau. \tag{D.12}$$

The solution of the equation of motion is the series given by Eq. (D.2) with the constants $c_{m,q}$ calculated based on the set of equations from Eq. (D.11).

References

[1] C. García, N. Dauchez, G. Lefebvre, Radiation efficiency of a distribution of baffled pistons with arbitrary phases, J. Acoust. Soc. Am. 152 (2) (2022) 1135–1145, http://dx.doi.org/10.1121/10.0013569.

[2] C. García A. N. Dauchez, G. Lefebvre, Modeling the acoustic radiation of plates using circular pistons, J. Sound Vib. 553 (9) (2023) 117656, http://dx.doi.org/10.1016/j.jsv.2023.117656.

[3] N. Hashimoto, Measurement of sound radiation efficiency by the discrete calculation method, Appl. Acoust. 62 (4) (2001) 429–446, http://dx.doi.org/10.1016/S0003-682X(00)00025-6.

[4] M.R. Bai, M. Tsao, Estimation of sound power of baffled planar sources using radiation matrices, J. Acoust. Soc. Am. 112 (3) (2002) 876–883, http://dx.doi.org/10.1121/1.1499133.

[5] J.P. Arenas, M.J. Crocker, Sound radiation efficiency of a baffled rectangular plate excited by harmonic point forces using its surface resistance matrix, Int. J. Acoust. Vib. 7 (4) (2002) 217–229, http://dx.doi.org/10.20855/ijav.2002.7.4120.

[6] J.P. Arenas, Numerical computation of the sound radiation from a planar baffled vibrating surface, J. Comput. Acoust. 16 (3) (2008) 321–341, http://dx.doi.org/10.1142/S0218396X08003671.

[7] J.P. Arenas, J. Ramis, J. Alba, Estimation of the sound pressure field of a baffled uniform elliptically shaped transducer, Appl. Acoust. 71 (2010) 128–133, http://dx.doi.org/10.1016/j.apacoust.2009.08.003.

[8] J. Zhong, X. Qiu, On the spherical expansion for calculating the sound radiated by a baffled circular piston, J. Theoret. Comput. Acoust. 30 (1) (2022) 2050026, http://dx.doi.org/10.1142/S2591728520500267.

[9] Y. Honda, H. Matsuhisa, S. Sato, Radiation efficiency of a baffled circular plate in flexural vibration, J. Sound Vib. 88 (4) (1983) 437–446, http://dx.doi.org/10.1016/0022-460X(83)90647-8.

[10] D.J. Hendy, Numerical evaluation of the sound power radiated from baffled, rectangular panels, J. Sound Vib. 127 (2) (1988) 283–289, http://dx.doi.org/10.1016/0022-460X(88)90303-3.

[11] G. Xie, D.J. Thompson, C.J.C. Jones, The radiation efficiency of baffled plates and strips, J. Sound Vib. 280 (2005) 181–209, http://dx.doi.org/10.1016/j.jsv.2003.12.025.

[12] Q. Li, D.J. Thompson, Directivity of sound radiated from baffled rectangular plates and plate strips, Appl. Acoust. 155 (2019) 309–324, http://dx.doi.org/10.1016/j.apacoust.2019.05.018.

[13] K. Sha, J. Yang, W.-S. Gan, A simple calculation method for the self-and mutual-radiation impedance of flexible rectangular patches in a rigid infinite baffle, J. Sound Vib. 282 (2005) 179–195, http://dx.doi.org/10.1016/j.jsv.2004.02.011.

[14] X. Zhang, W.L. Li, A unified approach for predicting sound radiation from baffled rectangular plates with arbitrary boundary conditions, J. Sound Vib. 329 (2010) 5307–5320, http://dx.doi.org/10.1016/j.jsv.2010.07.014.

[15] M. Karimi, L. Maxit, P. Croaker, O. Robin, A. Skvortsov, S. Marburg, N. Atalla, N. Kessissoglou, Analytical and numerical prediction of acoustic radiation from a panel under turbulent boundary layer excitation, J. Sound Vib. 479 (4) (2020) 115372, http://dx.doi.org/10.1016/j.jsv.2020.115372.

[16] C.W. Isaac, S. Wrona, M. Pawelczyk, N.B. Roozen, Numerical investigation of the vibro-acoustic response of functionally graded lightweight square panel at low and mid-frequency regions, Compos. Struct. 259 (1) (2021) 113460, http://dx.doi.org/10.1016/j.compstruct.2020.113460.

[17] T. Hasegawa, N. Inoue, K. Matsuzawa, A new rigorous expansion for the velocity potential of a circular piston source, J. Acoust. Soc. Am. 74 (3) (1983) 1044–1047, http://dx.doi.org/10.1121/1.389937.

[18] T.D. Mast, F. Yu, Simplified expansions for radiation from a baffled circular piston, J. Acoust. Soc. Am. 118 (6) (2005) 3457–3464, http://dx.doi.org/10.1121/1.2108997.

[19] L.L. Beranek, T.J. Mellow, Acoustics: Sound Fields, Transducers, and Vibration, Academic Press, London, 2019.

[20] W.P. Rdzanek, Sound scattering and transmission through a circular cylindrical aperture revisited using the radial polynomials, J. Acoust. Soc. Am. 143 (3) (2018) 1259–1282, http://dx.doi.org/10.1121/1.5025159.

[21] T. Mellow, L. Kärkkäinen, On the sound field of a circular membrane in free space and an infinite baffle, J. Acoust. Soc. Am. 120 (5) (2006) 2460–2477, http://dx.doi.org/10.1121/1.2354041.

[22] M. Greenspan, Piston radiator: Some extensions of the theory, J. Acoust. Soc. Am. 65 (3) (1979) 608–621, http://dx.doi.org/10.1121/1.382496.

[23] H. Levine, F.G. Leppington, A note on the acoustic power output of a circular plate, J. Sound Vib. 121 (2) (1988) 269–275, http://dx.doi.org/10.1016/S0022-460X(88)80029-4.

[24] W.P. Rdzanek, W.J. Rdzanek, Z. Engel, Theoretical analysis of sound radiation of an elastically supported circular plate, J. Sound Vib. 265 (2003) 155–174, http://dx.doi.org/10.1016/S0022-460X(02)01445-1.

[25] W.P. Rdzanek, W.J. Rdzanek, Asymptotic formulas for the acoustic radiation impedance of an elastically supported annular plate, J. Sound Vib. 301 (2007) 544–559, http://dx.doi.org/10.1016/j.jsv.2006.10.031.

[26] W.M. Zawieska, W.P. Rdzanek, W.J. Rdzanek, Z. Engel, Low frequency estimation for the sound radiation efficiency of some simply supported flat plates, Acta Acustica United Acustica 93 (2007) 353–363.

[27] W.P. Rdzanek, W.J. Rdzanek, K. Szemela, The low frequency axisymmetric modal sound radiation efficiency of an elastically supported annular plate, J. Sound Vib. 333 (2014) 144–165, http://dx.doi.org/10.1016/j.jsv.2013.09.004.

[28] W.P. Rdzanek, The acoustic power of a vibrating clamped circular plate revisited in the wide low frequency range using expansion into the radial polynomials, J. Acoust. Soc. Am. 139 (2016) 3199, http://dx.doi.org/10.1121/1.4954265, (2016).

[29] W.P. Rdzanek, Sound radiation of a vibrating elastically supported circular plate embedded into a flat screen revisited using the Zernike circle polynomials, J. Sound Vib. 434 (2018) 92–125, http://dx.doi.org/10.1016/j.jsv.2018.07.035.

[30] W.P. Rdzanek, K. Szemela, Sound radiation by a vibrating annular plate using radial polynomials and spectral mapping, J. Acoust. Soc. Am. 146 (2019) 2682, http://dx.doi.org/10.1121/1.5130193.

[31] A.D. Poularikas, Handbook of Formulas and Tables for Signal Processing, CRC Press, Boca Raton, 1998.

[32] A.W. Leissa, Vibration of Plates, Government Printing Office, Washington, 1969.

[33] F. Fahy, P. Gardonio, Sound and Structural Vibration: Radiation, Transmission and Response, second ed., Academic Press, New York, 2007.

[34] S.S. Rao, Vibration of Continuous Systems, John Wiley & Sons, New Jersey, 2007.